arXiv:1403.5728v1 [physics.space-ph] 23 Mar 2014

On the relationship between cosmic rays, solar activity and powerful earthquakes.

Kovalyov, M. (corresponding author)[1] and Kovalyov, S.[2]

[1]Sungkyunkwan University, South Korea, email: mkovalyo@ualberta.ca
[2]No affiliation

Abstract. In this paper we analyze the correlation of magnitude $\geqslant 7.8$ earthquakes to cosmic rays intensity. The correlation is far from simple and obvious but appears to hold for all but three earthquakes of magnitude $\geqslant 7.8$ since 1900. As a prequel to our study we analyze the correlation between the cosmic rays intensity and solar activity and its possible implications. We also show that magnitude $\geqslant 7.8$ earthquakes appear in groups; although the earthquakes of a group may appear in different places of the Earth, the time interval between two adjacent elements of the groups stays more or less the same.

§1. The cosmic ray intensity and sunspot numbers.

The relationship between the cosmic ray intensity (hereafter abbreviated as CRI) and the sunspot numbers (hereafter abbreviated as SSN) is well-known; high SSN correlates with low CRI, and vice versa as shown in Figure 1. The cosmic rays originate mainly outside of the Solar System, their intensity near Earth is currently believed to be modulated by cyclical solar activity with the average cycle of about 11 years long. We will refer to the eleven-year long cycles as *primary solar cycles* whenever there is a need to distinguish them from other cycles. The physical mechanism of the solar activity is unknown but is currently believed to be solely of purely solar origin.

A bit more careful analysis of Figure 1, however, shows that the maxima/minima of CRI lag the minima/maxima of SSN by a few months. The reason for the time lag is quite obvious and is explained in Figure 2.

It is currently believed that the solar activity modulates the flow of cosmic rays near the Earth but is not affected by them, which may not be the case. To understand why let us consider

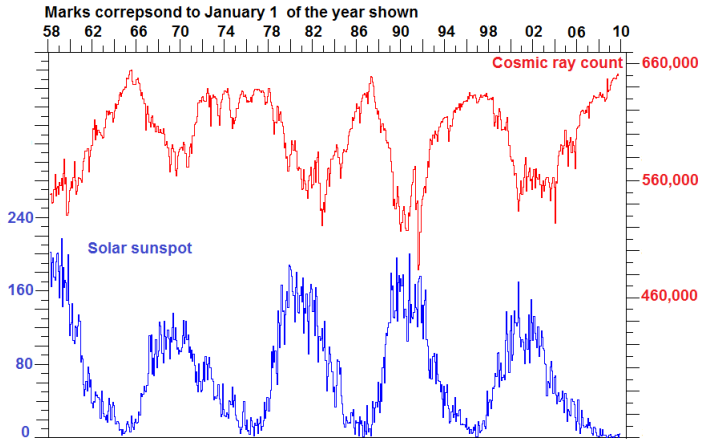

Figure 1: Monthly averages of CRI and SSN from 1958 to 2009 using data from the Germany Cosmic Ray Monitor in Kiel (GCRM) and NOAA's National Geophysical Data Center (NGDC), respectively. Source: [11].

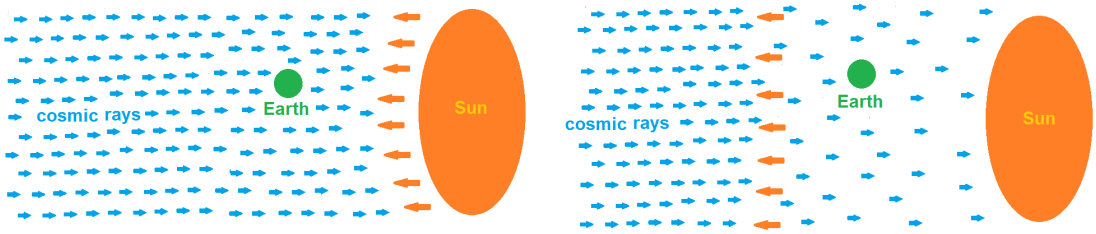

Figure 2: When SSN is at or just past a minimum (as shown on the left), the solar wind is present but weak and can deflect cosmic rays only near the Sun; by the time it reaches the Earth it loses its ability to deflect cosmic rays. It takes several months for the solar wind to gain sufficient strength to deflect cosmic rays for the time it takes it to reach the Earth. Hence the time lag between the maxima of CRI and the minima of SSN. The solar wind produced when SSN is at or just past a maximum (as shown on the right) is so strong that it can deflect cosmic rays for much longer than the time required to reach the Earth. As the solar wind passes the Earth and moves away from the Earth towards the interstellar space it continues to deflect cosmic rays thus reducing the amount of cosmic rays reaching the Earth for several more months. Hence the time lag between the minima of CRI and maxima of SSN. This is just a simplified picture with cosmic rays shown as flowing in one direction, the cosmic rays flow not from one but from all directions yet the flow is not isotropic.

an oversimplified thermal analogy roughly reflecting the interplay of cosmic rays and solar activity.

Thermal analogy of the interplay between cosmic rays and solar activity. Suppose we have a pot made of a complete thermal insulator; the pot is filled with a liquid and exposed to a rain of super-hot droplets. As more and more super-hot droplets fall into the pot the temperature of the liquid in the pot rises producing steam that goes up and deflects some super-hot droplets

while the rest of the super-hot droplets still fall in the pot. As the temperature of the liquid in the pot increases, so does the amount of steam and at some point in time there will be enough steam produced to deflect all but a few super-hot droplets. As only a few super-hot droplets fall into the pot, the temperature of the liquid in the pot reaches its maximum and begins to decrease. As the temperature of the liquid in the pot decreases, so does the amount of steam; with the amount of steam decreasing more and more super-hot droplets avoid deflection by the steam and fall into the pot. As the temperature of the liquid in the pot continues to decrease so does the amount of steam, resulting in fewer and fewer super-hot droplets getting deflected and more and more of them falling into the pot. At some point in time there will be so many super-hot droplets falling into the pot that the temperature of the liquid in the pot will begin to increase again and the process will repeat itself over and over again. As the process repeats itself, the amount of steam will periodically increase and decrease and so will the number of super-hot droplets falling into the pot; when the amount of steam increases, the number of super-hot droplet falling into the pot decreases and vice versa. But if the rain of super-hot droplets completely stops, the steam will also completely stop. The super-hot droplets correspond to cosmic rays, steam corresponds to solar wind and the pot with liquid corresponds to the Sun, bubbles in the liquid in the pot correspond to sun spots. The similarity is illustrated in Figure 3. The example does not reflect the reversal of the solar magnetic field about every 11 years.

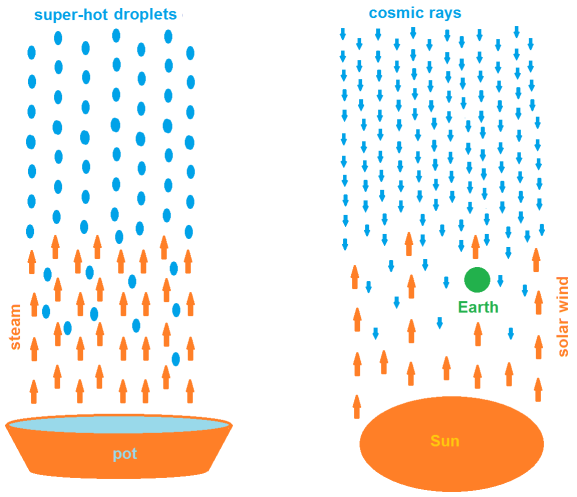

Figure 3: Illustration of the oversimplified thermal analogy of the interplay between cosmic rays and solar activity.

Contrary to the currently accepted views, the example suggests that the cosmic rays might be the very source of the solar activity, just like the super-hot droplets are the source of the rise in temperature in the pot. The analogy also suggests that if the flow of cosmic rays, reflected by CRI, was reduced to almost zero, so would be the solar activity reflected by SSN. If the rain of super-hot droplets in the example continued for a long time at a high level, the liquid in the pot would evaporate leading to a prolonged period without steam. In a similar manner we may guess that if the flow of the cosmic rays continued at a high level for sufficiently long time, the solar activity would drop down and stay low for a considerable period of time; we shall call such an event a *burn-out*.

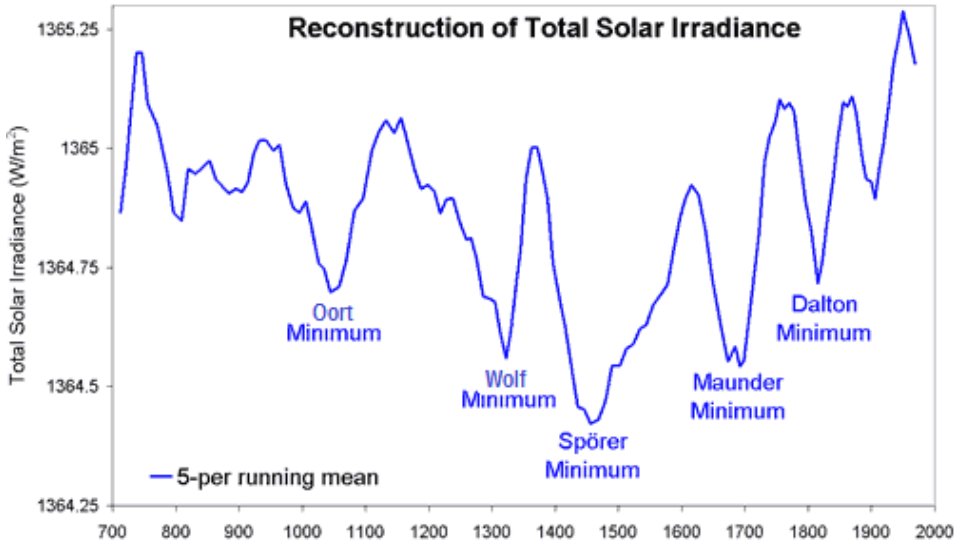

Figure 4: Solar activity for the past 1300 years as represented by total solar irradiance, reconstructed based on ^{10}B . Source: [3].

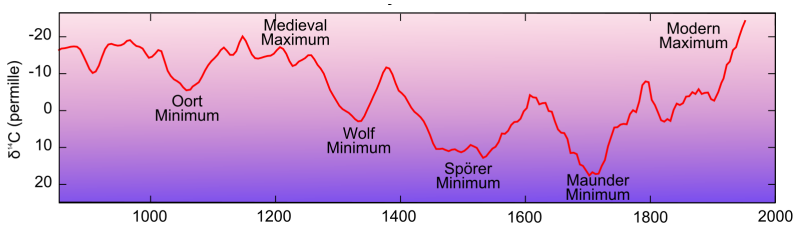

Figure 5: Solar activity for the past 1200 years, reconstructed based on ^{14}C . Source: [7].

Figures 4, 5 show reconstructed solar activity for the past millennium. Figure 4 shows

remarkable similarity between the left and right halves of the graph. So in Figure 6 we superimpose the graph from Figure 4 shown in blue; its horizontally flipped image shown in red; and two green curves, the one on the left is part of the blue curve, the one on the right is the horizontally flipped image of the green curve on the left. The green curves are inserted to illustrate that the period between the Dalton and Maunder Minima is actually two secondary solar cycles blended together, and so is the period between the Wolf and Oört Minima. The whole graph shows 11 secondary cycles of solar activity, each about 118 years or about 11 primary solar cycles long. Article [3] also mentions that [6] predicts the existence of a secondary maximum centered around year 1220 AD and the Dome Fuji record features a secondary peak between 1570 and 1600 AD, confirming our hypothesis that the periods between the Oort and Wolf Minima and between the Spörer and Maunder Minima contain two rather than one primary solar cycles merged together. The 118-year length of secondary solar cycles is supported by [8] which discusses evidence of the existence of 60-year (about half of 118 years) long cycles in nature. The 118-year length of the secondary solar cycle might be the reason why the Chinese zodiac is comprised of 12 (about one tenth of 118) signs and why the Chinese time counting involves 60-year (about half of 118) cycles.

Figure 7, although considerably different, also suggests the existence of secondary cycles of about 118-year length; the broken lines show that some cyclic activity that seems to be "missing".

The presence of secondary solar cycles in Figures 6,7 suggests that an important component of cosmic rays comes from one or several distinct source(s), whose cyclical motion accounts for the 118-year cycles.

The dotted curves in Figure 7 indicate the change in the solar activity observed on Earth attributed to the changing strength of the Earth's own magnetic field. However, the change in the strength of the Earth's magnetic field itself might be due to the change in CRI. After all, cosmic rays is a current of electrically charged particles which generates a magnetic field that interacts with the currents of electrically charged liquid metal inside the Earth's liquid core responsible for the Earth's magnetic field.

The argument presented here might be considered contrary to the point of view that the cosmic rays are isotropic in their arrival directions. Yet it is not. On a very cloudy and foggy day the sunlight arrives from the direction of the Sun, but to an observer on the Earth the light appears to arrive from all directions due to scattering by the clouds and fog. In the same manner the cosmic

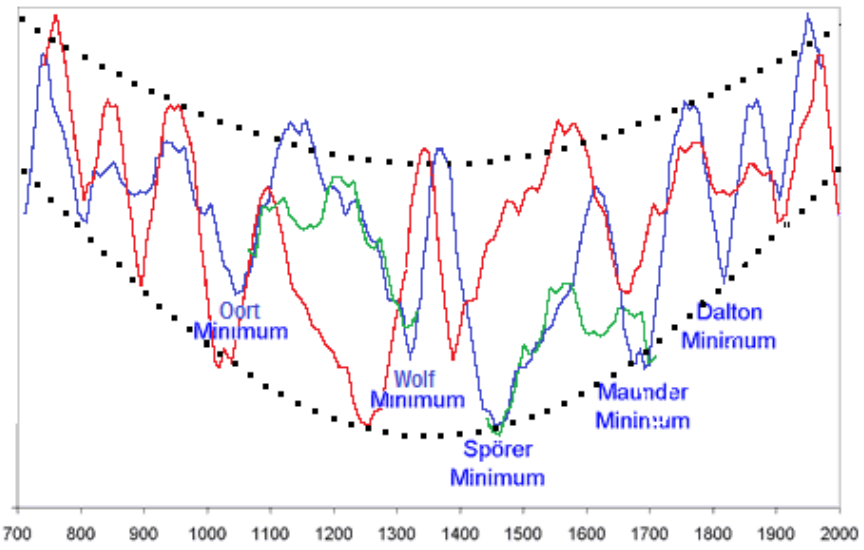

Figure 6: Figure 4 with red and green curves superimposed on it. The red curve is the horizontally flipped image of the blue curve in Figure 4, the green curve on the left is part of the blue curve, the green curve on the right is the horizontally flipped image of the green curve on the left. The green curves are inserted to illustrate that the period between the Dalton and Maunder Minima solar cycles is actually two secondary solar cycles blended together, and so is the period between the Wolf and Oort Minima.

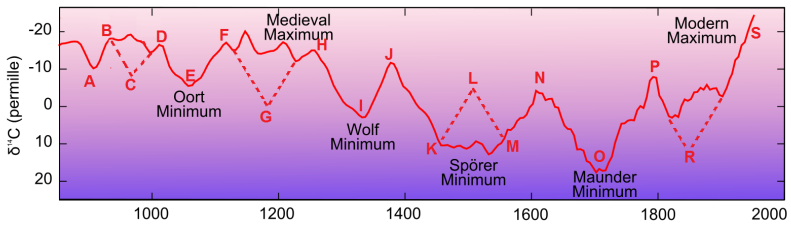

Figure 7: Same graph as in Figure 7 with broken lines indicating activity that seemingly should have occurred but did not.

rays arriving from a single source may appear to arrive from all directions due to scattering by interstellar and galactic gases; electromagnetic and gravitational fields; and, in no small part, the solar wind. The presence of a small anisotropy is discussed in [1, 2].

In favor of our hypothesis that cosmic rays are behind the solar cycles also speaks [5]. The authors looked at the records of geomagnetic activity stretching back almost 150 years and noticed that the geomagnetic activity foretells what the solar cycle is going to be like 6-8 years in the future. Their prediction that the peak of the current solar cycle will be one of the most intense since record-keeping began almost 400 years ago seems to have failed spectacularly. Their main

idea that the value of a local maximum of a long-term average R of SSN is correlated to the value of the preceding local maximum of $\mathrm{IHV_I}$ is illustrated in Figure 8. But did they really fail? We believe not. If, indeed, the solar and terrestrial activities are influenced by cosmic rays as illustrated by the over-simplified analogy earlier, then it would certainly take much longer for the Sun to react to an increase/decrease in CRI than it would take the Earth for the same reason it takes longer to boil a large pot of water than a small one. Thus the changes in solar activity should be expected to be preceded by corresponding changes in terrestrial activities. While the value of IHV (Inter-hour Variability Index) reflects the value of CRI at about the same time, the value of a local maximum of the long-term average of SSN shown in Figure 8 most likely reflects the cumulative effect of CRI given by the integral of CRI over the preceding solar cycle. Consequently the value of SSN should be correlated not with IHV but rather with the integral of IHV over the preceding solar cycle. A quick look at Figure 8 shows that the graph of IHV from about 2001 is very narrow and thus the integral of IHV is quite small foretelling a rather small maximum of the current solar cycle. Another correlation between the solar and geomagnetic activities is shown in Figure 9, where the minima of IHV seem to follow the same pattern as the maxima of SSN. The exact relationship between IHV, SSN and CRI is far from clear; although predictions of SSN based on IHV are possible, it might take a century or so of observations and comparisons before reliable predictions can be made.

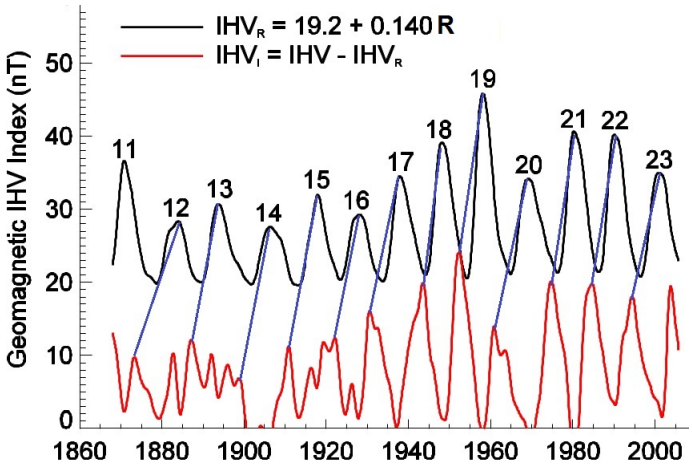

Figure 8: Solar cycles vs geomagnetic activity. Peaks in geomagnetic activity (as measured by $\mathrm{IHV_I}$) shown in red foretell solar maxima shown in black (measured by a long-term average of SSN denoted by R) 6-8 years in advance. The numbers at the maxima of the solar cycles are the *solar cycle numbers*. Source: [5].

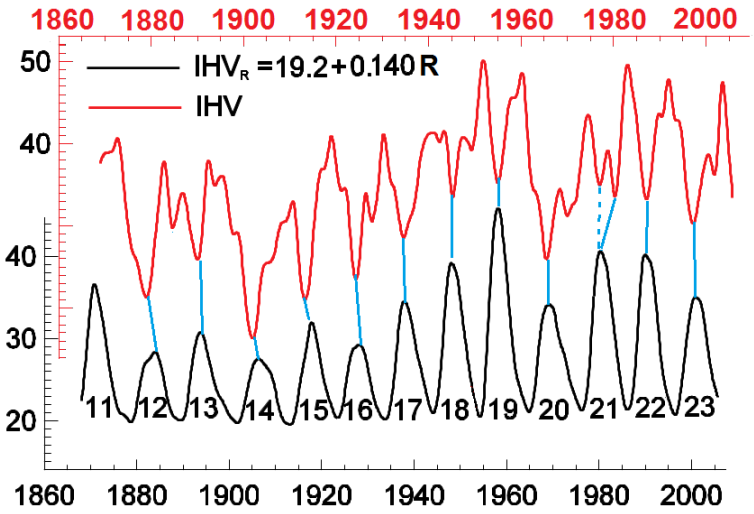

Figure 9: Solar cycles vs geomagnetic activity. The black graph with black axes and labels shows $\mathrm{IHV_R}$ representing the solar activity, the numbers at the base of the solar cycles are the *solar cycle numbers* and R is a long-term average of SSN. The red graph with red axes and labels shows IHV representing geomagnetic activity. Notice the red graph is shifted right by about 30 months. The minima in geomagnetic activity as measured by IHV foretell solar maxima about 20-30 months in advance for all but one solar maximum, the minima of IHV are connected to the corresponding maxima of $\mathrm{IHV_R}$ by solid blue lines. The only exception is solar cycle 21, its maximum was only about one month after the corresponding minimum of IHV, yet there was one more local minimum of IHV preceding the solar maximum and it was 20-30 months ahead of the solar maximum. Source: [4].

§2. Correlation between magnitude $\geqslant 7.8$ earthquakes and CRI/SSN.

In this section we restrict our attention to earthquakes of magnitude $\geqslant 7.8$ since 1900, these are the most powerful earthquakes, crème de la crème of natural disasters. The list of the earthquakes was obtained by taking all earthquakes of magnitude $\geqslant 8.0$ from [10] and supplementing with the magnitude $7.8-7.9$ from [9]. Although both web sites are produced by USGS, some of the earthquakes are assigned different magnitude and/or different date, albeit the differences are rather insignificant for our purposes. Sifting through the two lists double entries as well as aftershocks and foreshocks were removed, dates and magnitudes were adjusted based on additional sources. The earthquakes of magnitude $\geqslant 8.0$ since 1900 are listed in the appendix to this article along with some additional information about them.

In Figure 10 earthquakes of magnitude $\geqslant 7.8$ from 1958 to 2010 are superimposed on the

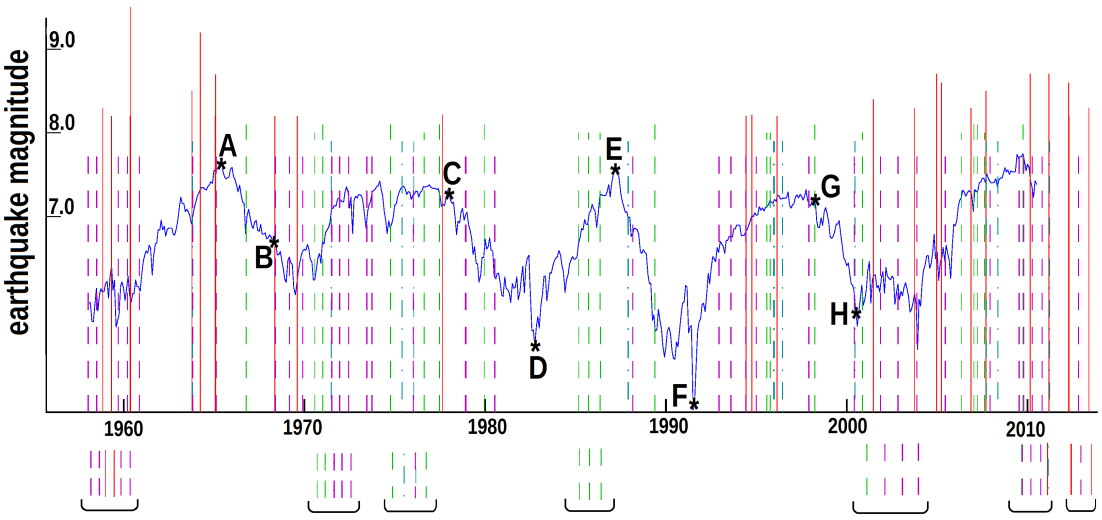

Figure 10: CRI vs earthquakes. Red solid vertical lines represent earthquakes of magnitude > 8.1 , green broken vertical lines represent earthquakes of magnitude 8.0 and 8.1, green dot-dash vertical lines represent earthquakes of magnitude 7.9, and purple broken vertical lines represent earthquakes of magnitude 7.8. The blue curve is the CRI intensity from Figure 1. Several groups of earthquakes are shown under the main graph.

graph of CRI from Figure 1. One may notice the following.

1. The powerful earthquakes are much less frequent when the CRI decreases, i.e in the periods between A and B, C and D, E and F, G and H. There is only one earthquake between A and B and that earthquake happened when CRI dropped down and then rose up sharply; there are only three earthquakes between C and D and the first two happened shortly after CRI dropped down and then rose up sharply; there are only three earthquakes between E and F and the first two happened shortly after CRI dropped down and then rose up sharply. That leads us to conjecture that high magnitude earthquakes are correlated to the change in CRI, specifically they are somehow caused or amplified when the rate of change of CRI is > 0 .

2. Figure 10 shows five CRI cycles. Two CRI cycles, specifically 1961-1968 and 1982-1991, have triangular graphs and correspond to considerably fewer powerful earthquakes than the other three.

3. The powerful earthquakes are much less frequent at the time when the graph of CRI is more or less like a straight line, i.e. prior to point A, between A and B, between C and D, between D and E, between E and F, between G and H; and more frequent on at the time when the graph of CRI is very much like a curve convex up, i.e. between B and C, between F and G, beyond H. That

leads us to conjecture that high magnitude earthquakes are correlated to the second derivative of a certain long-term average of CRI, specifically they are somehow caused or amplified when the second derivative of a certain long-term average of CRI is < 0 .

4. One may also notice that some high magnitude earthquake come in groups, with about the same time interval between adjacent elements of the group.

There are no reliable CRI records for the period 1900-1958, however there are reliable records of SSN which may be used as a proxy for CRI while keeping in mind that CRI lags SSN by a few months.

In Figures 11, 12, 13 we superimpose magnitude $\geqslant 7.8$ earthquakes on the graphs of SSN. We see the presence of earthquakes groups just like in Figure 10. The earthquakes are much less frequent where CRI decays or, equivalently, SSN increases. There are two earthquakes between 1915 - early 1916, three earthquakes in late 1935 - early 1936, one earthquake in 1966, one earthquake in 1988, one earthquake in 1998 and a double earthquake in the beginning of 2011 which appear at the very beginning of increasing stages of SSN; yet due to the lag of SSN behind CRI these earthquakes are at maxima of CRI rather than the decreasing stages. There are three earthquakes in late 1935 - early 1936, one earthquake in 1956 and one in 1978 at increasing stages of SSN yet SNN drops for 3-4 months prior to each earthquake exhibiting behavior of being at a decreasing rather than increasing stage of a cycle.

The four earthquakes: November 27, 1945, Pakistan; April 1, 1946, Alaska; August 4, 1946, Hispaniola; December 21, 1946, Japan; are somewhat of a mystery. The first one was at a maximum of CRI and was preceded by a decrease in SSN/increase in CRI so it fits the pattern. However the other three were at an increasing stage of SSN/decreasing stage of CRI whose presence cannot be easily explained: they are too far from the beginning of the SNN minimum/CRI maximum to be explain by the time lag nor were they preceded by short-term decreases. These are the only three out of about 170 earthquakes, foreshocks and aftershocks of magnitude $\geqslant 7.8$ which appear at an increasing stage of SNN/decreasing stage of CRI. What makes them even more mysterious is that the time intervals between the four earthquakes are correspondingly 125, 125, and 139 days, that is about the same, even though they were spread out all over the planet. Yet there seems to be nothing special about the 1945 - 1946 years, except that those were the years of the first nuclear weapon testing; it is very doubtful nuclear testing could have contributed to the four high

magnitude earthquakes.

Conclusion.

We have shown here that the earthquakes of magnitude $\geqslant 7.8$ since 1900 are correlated with CRI. Of all such earthquakes only three seem to be at the time of decreasing CRI; the rest are either at CRI minima/maxima or coincide with an increase in CRI, the increase may be either of a short-term or prolonged nature. What causes such correlation is not clear but it cannot be just coincidental. Nor is it clear whether the cosmic rays cause high-magnitude earthquakes or merely amplify their power.

It is currently believed that SSN modulates CRI, yet this article points out that the very source of the variability in solar activity might be the cosmic rays themselves. Although the primary solar cycles and their $\approx 11-$ year length are most likely of solar origin, the secondary cycles in solar activity, as well as non-cyclical changes, are most likely of extra-solar origin. It seems that earthquakes, and possibly Earth's climate, are affected by events taking place far away from the Solar System. The change in the Earth's own magnetic field, including the polarity reversal, might also be due to the ever changing flow of cosmic rays.

Figures 6, 7 suggest that we have reached the maximum in the secondary solar cycle and are heading towards the next minimum, the amplitudes of the primary solar cycles will be decreasing albeit non-monotonically. If we are correct, we can expect temperatures to decrease for the next 50-60 years and the number of high-powered earthquakes to increase.

Appendix. Magnitude $\geqslant 8.0$ earthquakes since 1900.

The set of earthquakes below is based on [10]. The letter "p" after the sequential number indicates an increase in the lunar or solar gravity pull due to temporal proximity to a New/Full Moon, sequence of dates when New/Full Moon coincided with or was close to a perigee, temporal proximity to perihelion, etc. In this article "New Moon" means the Moon at most 2% visible and "Full Moon" means the Moon at least 98% visible.

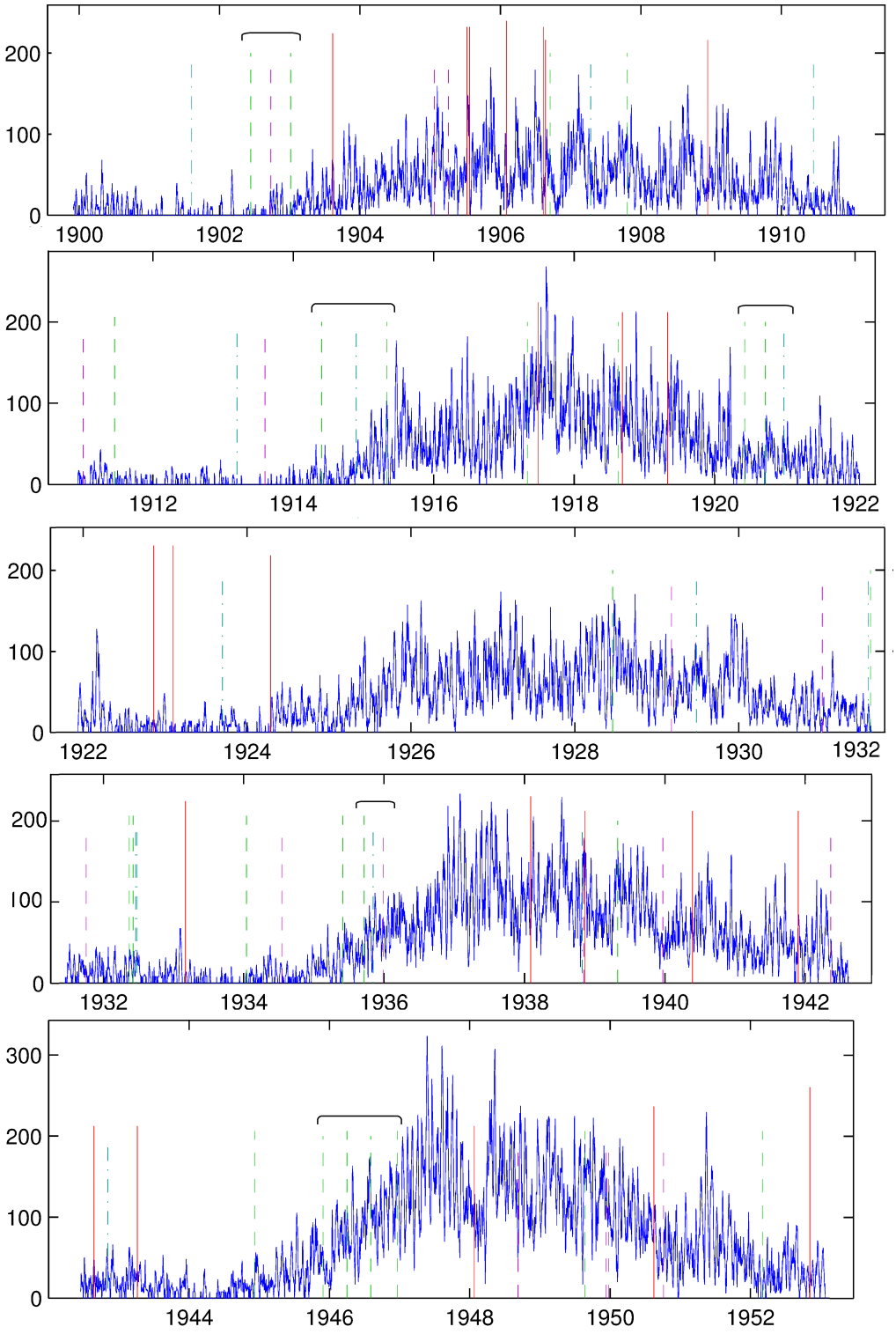

Figure 11: SSN vs earthquakes from January 1, 1900 to August 15, 1942. Notations are explained in the caption to Figure 13.

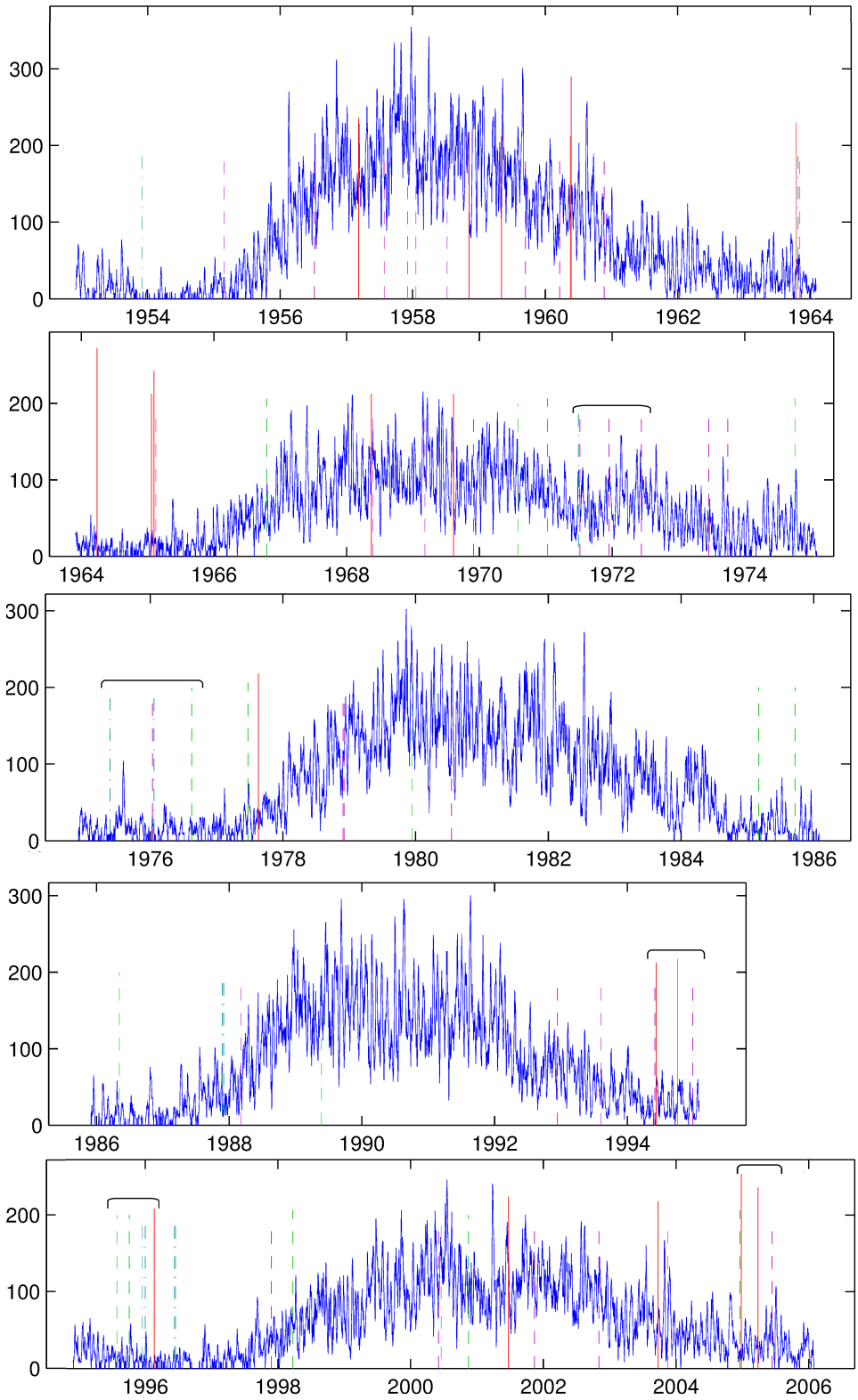

Figure 12: SSN vs earthquakes August 16, 1942 to December 31, 1985. Notations are explained in the caption to Figure 13.

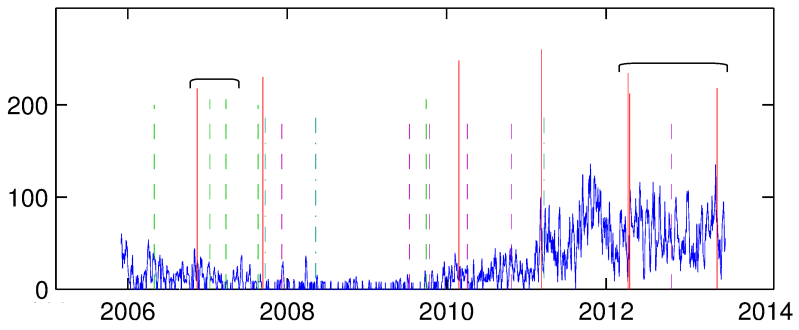

Figure 13: SSN vs earthquakes from January 1, 1986 to June 30, 2013. Red solid vertical lines represent earthquakes of magnitude > 8.1 , green broken vertical lines represent earthquakes of magnitude between 8.0 and 8.1, green dot-dash vertical lines represent earthquakes of magnitude 7.9, and purple broken vertical lines represent earthquakes of magnitude 7.8; the length of each vertical line represents the magnitude of the corresponding earthquake. The blue curve is daily SSN. Horizontal brackets cover either groups of earthquakes with the time between the adjacent elements of the group to be about the same, or sets of earthquakes containing such groups.

Of the 92 earthquakes listed below, 70 (76%) had some sort of increase in gravitational pull prior or close to them, suggesting that the combined lunar-solar gravitational pull does play a certain role in the Earth's seismic activity. Since the Earth's liquid core is liquid it is subject to the tidal motion just like water on the Earth's surface. Unlike water on the surface, the liquid metal in the liquid core cannot freely move up or down; instead the pressure exerted from the liquid core on the mantle changes depending on the combined lunar-solar gravitational pull. Such changes influence the motion of the mantle contributing to earthquakes. Also unlike water on the Earth's surface the liquid core contains electrical currents within it which are affected by the flow of cosmic rays. The magnetic field created by cosmic rays makes the currents within the liquid core move, not much differently from the lunar-solar gravitational pull, contributing to Earth's seismic activity.

1p) June 11, 1902, Okhotsk Sea, M=8.0. Preceded by June 6 New Moon-perigee, May 8 New Moon-perigee. Solar minimum.

2p) January 4, 1903, Tonga, M=8.0. Coincided with perihelion, preceded by December 29 New Moon, December 15 Full Moon-perigee with the perigee being the closest of the year, November 17 Full Moon-perigee. Solar minimum.

3p) August 11, 1903, Greece, M=8.3. Preceded by August 9 Full Moon, July 24 New Moon-perigee, June 26 New Moon-perigee. Solar minimum.

4) July 9, 1905, Mongolia, M=8.4.

5) July 23, 1905, Mongolia, M=8.4.

6p) January 31, 1906, Ecuador-Columbia, M=8.8. Close to February 1 50% Moon-apogee (combined gravitational pull of the Sun and Moon at its weakest), preceded by January 23 New Moon - January 20 perigee, January 9 Full Moon - January 3 perihelion, December 26 New Moon - December 23 perigee, November 25 New Moon-perigee. Local minimum within a solar maximum.

7p) August 17, 1906, M=8.2. Close to August 19 New Moon.

8p) October 21, 1907, Afghanistan, M=8.0. Coincided with Full Moon.

9) December 12, 1908, Peru, M=8.2. Local minimum within a solar maximum.

10p) June 15, 1911, Japan, M=8.1. Preceded by June 11 Full Moon, May 28 New Moon-perigee, April 29 New Moon - April 30 perigee. Solar minimum.

11p) May 26, 1914, New Guinea, M=8.0. Preceded by May 25 New Moon, May 8 Full Moon-perigee, April 10 Full Moon-perigee with the perigee being the closest of the year, March 12 Full Moon-perigee. Solar minimum.

12p) May 1, 1915, Kuril Islands, M=8.0. Preceded by April 30 Full Moon-perigee, April 1 Full Moon-perigee. Solar minimum.

13) May 1, 1917, New Zealand, M=8.0.

14) June 26, 1917, Tonga, M=8.4.

15) August 15, 1918, Celebes Sea, M=8.0.

16p) September 7, 1918, Kuril Islands, M=8.2. Preceded by September 6 New Moon.

17p) April 30, 1919, Tonga, M=8.2. Coincided with April 30 New Moon-perigee, preceded by April 1 New Moon-perigee.

18p) June 5, 1920, Taiwan, M=8.0. Preceded by June 1 Full Moon, May 19 New Moon-perigee. Solar minimum.

19) September 20, 1920, Loyalty Islands, M=8.0. Solar minimum.

20p) November 11, 1922, Chile-Argentina Border, M=8.5. Preceded by October 19 New Moon-perigee, September 21 New Moon-perigee, August 23 New Moon-perigee. Solar minimum.

21p) February 3, 1923, Kamchatka, M=8.5. Coincided with February 2 Full Moon - February 4 perigee, preceded by January 3 Full Moon - January 2 perihelion. Solar minimum.

22) April 14, 1924, Philippines, M=8.3. Solar minimum.

23p) June 17, 1928, Mexico, M=8.0. Coincided with June 17 New Moon - June 16 perigee, May 19 New Moon-perigee, April 20 New Moon-perigee. Solar maximum.

24) August 10, 1931, Xinjiang, China, M=8.0. Solar minimum.

25p) June 3, 1932, Mexico, M=8.1. Coincided with New Moon, preceded by May 19 Full Moon-perigee, April 20 Full Moon-perigee with the perigee being the closest of the year. Solar minimum.

26) March 2, 1933, Sanriku, Japan, M=8.4. Solar minimum.

27p) January 15, 1934, India, M=8.1. Coincided with January 15 New Moon-perigee, preceded by December 17 New Moon-perigee, January 1 Full Moon - January 2 perihelion. Solar minimum.

28p) May 31, 1935, Pakistan, M=8.1. Close to June 1 New Moon. Solar minimum.

29p) September 20, 1935, Papua New Guinea, M=8.1. Preceded by September 12 Full Moon-perigee with the perigee closest of the year, August 15 Full Moon-perigee. Solar minimum.

30p) February 1, 1938, Banda Sea, Indonesia, M=8.5. Coincided with New Moon, preceded by January 15 Full Moon-perigee, December 17 Full Moon-perigee, November 19 Full Moon-perigee, January 2 New Moon - January 3 perihelion.

31p) November 10, 1938, Shumagin Islands, Alaska, M=8.2. Coincided with November 8 Full Moon - November 11 perigee.

32) April 30, 1939, Solomon Islands, M=8.0. Preceded by April 28 perigee.

33p) May 24, 1940, Peru, M=8.2. Preceded by May 20-22 Full Moon - May 18 perigee, April 21 Full Moon-April 20 perigee, March 23 Full Moon-perigee with the perigee being the closest of the year, February 23 Full Moon-perigee, January 24 Full Moon - January 23 perigee.

34p) November 25, 1941, Azores-Cape St. Vincent Ridge, M=8.2. Preceded by November 19 New Moon-perigee, with the perigee being the closest of the year.

35p) August 24, 1942, Peru, M=8.2. Coincided with August 25 Full Moon - August 23 perigee, preceded by July 26 Full Moon - perigee, June 28 Full Moon-perigee, May 30 Full Moon-perigee with the perigee being the closest of the year. Solar maximum.

36p) April 6,1943, Chile, M=8.2. Preceded by April 5 New Moon, March 5 New Moon - March 4 perigee, February 4 New Moon-perigee, January 6 New Moon-perigee, December 8 New Moon -perigee. Solar minimum.

37) December 7, 1944, Japan, M=8.1. Solar minimum.

38p) November 27, 1945, Pakistan, M=8.0. Preceded by November 19 Full Moon-perigee, October

21 Full Moon-perigee with the perigee being the closest of the year, September 23 Full Moon-perigee. Solar minimum.

39p) April 1, 1946, Alaska, M=8.1. Coincided with April 1-2 New Moon - April 3 perigee.

40) August 4, 1946, Dominican Republic, M=8.0.

41p) December 21, 1946, Japan, M=8.1. Close to December 22 New Moon, January 4 perihelion.

42p) January 24, 1948, Philippines, M=8.2. Close to January 25 Full Moon - January 26 perigee, with the perigee closest in the year; preceded by December 28 Full Moon-perigee, January 2 perihelion. Local minimum in the middle of a solar maximum.

43p) August 22, 1949, B.C., Canada, M=8.1. Close to August 23-24 New Moon - August 25 perigee.

44p) August 15, 1950, Assam, Tibet, M=8.6. Preceded by August 14 New Moon.

45) March 4, 1952, Japan, M=8.1. Solar minimum.

46p) November 4, 1952, Kamchatka, M=9.0. Preceded by November 2 Full Moon - October 29 perigee - November 1 solar flare, October 2 Full Moon - October 1 perigee, September 3 Full Moon-perigee, August 5 Full Moon-perigee, July 8 Full Moon-perigee with August 5 being the closest perigee of the year. Solar minimum.

47p) March 9, 1957, Andreanof Islands, Alaska, M=8.6. Preceded by February 14 Full Moon-perigee, January 16 Full Moon-perigee, December 18 Full Moon -December 19 perigee, January 2 New Moon - January 3 perihelion. Local minimum inside a solar maximum.

48p) December 4, 1957, Mongolia, M=8.1. Close to December 6 Full Moon.

49p) November 6, 1958, Kuril Islands, M=8.3. Close to November 10 New Moon-perigee, preceded by October 13 New Moon-perigee, September 14 New Moon-perigee.

50) May 4, 1959, Kamchatka, M=8.2.

51p) May 22, 1960, Chile, M=9.5-9.6; this is the most powerful earthquake in known history. Preceded a day earlier by a M=7.9-8.2 foreshock. Preceded by May 12 Full Moon-perigee; close to May 24 New Moon. Preceded by the largest known solar maximum of 1958 and by the largest known value in IHV, see Figure 9.

52) October 13, 1963, Kuril Islands, M=8.5. Solar minimum.

53p) March 28, 1964, Alaska, M=9.2. Coincided with March 28 Full Moon. Solar minimum.

54p) February 4, 1965, Alaska, M=8.7. Preceded by February 2 New Moon, January 17 New

Moon-perigee, December 19 Full Moon -perigee, November 19 Full Moon - November 20 perigee, December 19 Full Moon-perigee with the perigee being the closest of the year, January 2 New Moon-perihelion. Solar minimum.

55p) October 17, 1966, Peru, M=8.1. Preceded by October 13 New Moon-perigee, September 14 New Moon-perigee, August 17 New Moon-perigee.

56p) May 16, 1968, Honshu, Japan, M=8.2. Preceded by May 12 Full Moon-perigee, April 13 Full Moon - April 14 perigee. Solar maximum.

57p) August 11, 1969, Kuril Islands, M=8.2. Close to August 12 New Moon, preceded by July 28 Full Moon-perigee, July 29 Full Moon-perigee with the perigee being the closest of the year, June 1 Full Moon-perigee. Solar maximum.

58p) July 31, 1970, Colombia, M=8.0. Close to August 1 New Moon.

59p) January 1, 1971, Indonesia, M=8.1. Coincided with December 28 Full Moon - December 31 perigee-January 4 perihelion.

60p) October 3, 1974, Peru, M=8.1. Preceded by October 2 Full Moon, September 15 Moon - September 14 perigee, August 17 New Moon-perigee, July 19 New Moon-perigee. Solar minimum.

61) August 16, 1976, Philippines, M=8.0.

62p) June 22, 1977, Tonga, M=8.1. Preceded by June 17 New Moon, June 1 Full Moon-perigee, May 4 Full Moon-perigee. Solar minimum.

63p) August 19, 1977, Indonesia, M=8.3. Preceded by August 12 New Moon, July 29 Full Moon - July 28 perigee, June 29 Full Moon-perigee, June 1 Full Moon-perigee, May 4 Full Moon-perigee. Solar minimum.

64) December 12, 1979 Ecuador, M=8.1. Solar minimum.

65) March 3, 1985, Chile, M=8.0. Solar minimum.

66p) September 19, 1985, Mexico, M=8.0. Preceded by September 15 New Moon. Solar minimum.

67p) May 7, 1986, Alaska, M=8.0. Coincided with New Moon. Solar minimum.

68p) May 23, 1989, Macquarie Island, M=8.1. Preceded by May 21 Full Moon, May 4 New moon-perigee, April 5 New Moon-perigee, March 8 New Moon-perigee. Local minimum in a solar maximum.

69p) June 9, 1994, La Paz, Bolivia, M=8.2. Coincided with New Moon, preceded by May 24 Full Moon-perigee, April 25 Full Moon-perigee with the perigee being the closest of the year, March 25

Full Moon-perigee. Solar minimum.

70p) October 4, 1994, Kuril Islands, M=8.3. Coincided with October 4-5 New Moon - October 6 perigee, September 6 New Moon-perigee.

71p) July 30, 1995, Chile, M=8.0. Coincided with July 11 Full Moon-perigee, June 13 Full Moon-perigee with the perigee being the second closest of the year, May 15 Full Moon-perigee. Solar minimum.

72p) October 9, 1995, Mexico, M=8.0. Coincided with Full Moon. Solar minimum.

73p) February 17, 1996, Indonesia, M=8.2. Coincided with February 18 New Moon - February 17 perigee, preceded by January 19 New Moon-perigee, December 22 New Moon-perigee. Solar minimum.

74p) March 25, 1998, Balleny Islands, M=8.1. Close to March 28 New Moon-perigee, preceded by February 27 New Moon-perigee, January 29 New Moon - January 30 perigee.

75) November 16, 2000, Papua New Guinea, M=8.0. Solar maximum.

76p) June 23, 2001, Peru, M=8.4. Coincided with June 22 New Moon - June 23 perigee. Local minimum in a solar maximum.

77p) September 25, 2003, Japan, M=8.3. Coincided with September 25 New Moon - September 28 perigee.

78p) December 23, 2004, Macquarie Island, M=8.1. Close to December 26 Full Moon; preceded by December 12 New Moon-perigee, close to January 2 perihelion. Solar minimum.

79p) December 26, 2004, Sumatra, Indonesia, M=9.1. Coincided with Full Moon; preceded by December 12 New Moon-perigee, November 13 New Moon - November 12 perigee, close to January 2 perihelion and January 10 New Moon-perigee with the perigee being the closest for 2004-05. Solar minimum.

80p) March 28, 2005, Sumatra, Indonesia, M=8.6. Preceded by March 26 Full Moon, February 7 New Moon-perigee, January 10 New Moon-perigee-January 2 perihelion, December 12 New Moon-perigee. Solar minimum.

81) May 3, 2006, Tonga, M=8.0.

82p) November 15, 2006, Kuril Islands, M=8.3. Coincided with apogee. Preceded by November 4 Full Moon - November 3 perigee, October 6 Full Moon-perigee, September 8 Full Moon-perigee, August 10 Full Moon-perigee. Solar minimum.

83p) January 13, 2007, Kuril Islands, M=8.1. Preceded by January 3 Full Moon-perihelion. Solar minimum.

84p) April 1, 2007, Solomon Islands, M=8.1. Coincided with Full Moon; preceded by March 19 New Moon-perigee. Solar minimum.

85) August 15, 2007, Peru, M=8.0. Solar minimum.

86p) September 12, 2007, Indonesia, M=8.5. Coincided with New Moon. Solar minimum.

87p) September 29, 2009, Samoa, M=8.1. Preceded by September 27 Full Moon - September 28 perigee, one month prior to the closest perigee of the year. Solar minimum.

88p) February 27, 2010, Maule, Chile, M=8.8. Coincided with February 27 Full Moon-perigee, preceded by January 30 Full Moon-perigee, December 31 Full Moon - January 1 perigee - January 3 perihelion. Solar minimum.

89p) March 11, 2011, Honshu, Japan, M=9.0. Preceded by February 19 Full Moon-perigee, January 4 Full Moon - January 3 perihelion.

90p) April 11, 2012, Sumatra, Indonesia, M=8.6, followed by an M=8.2 aftershock. Preceded by April 7 Full Moon-perigee one month prior to the closest perigee of the year, March 9 Full Moon - March 10 perigee. Local minimum in a solar maximum.

91p) April 11, 2012, Sumatra, Indonesia, M=8.2. This earthquakes struck just just 2 hours 7 minutes after 8.6 earthquake. Preceded by April 7 Full Moon-perigee one month prior to the closest perigee of the year, March 9 Full Moon - March 10 perigee. Local minimum in a solar maximum.

92p) May 24, 2013, Okhotsk Sea, M=8.3. Coincided with May 24 Full Moon - May 26 perigee one month prior tot he closest perigee of the year, April 26 Full Moon - April 28 perigee. Local minimum in a solar maximum.

Acknowledgments.

The pictures/graphs used in this article were either reproduced from public domains with references provided or with permission of the creator(s), the authors would like to express their gratitude to all those who created the pictures and those who made them available to the public.

References

[1] Abbasi, R.et al. Measurement of the anisotropy of cosmic-ray arrival directions with icecube, *The Astrophysical Journal Letters*, 718, l194. 2010. http://iopscience.iop.org/2041-8205/718/2/L194.

[2] Abbasi, R.et al. Observation of an anisotropy in the galactic cosmic ray arrival direction at 400 tev with icecube. 2012. http://arxiv.org/abs/arXiv:1109.1017.

[3] Delaygue, G., Bard, E. An Antarctic view of Beryllium-10 and solar activity for the past millennium, *Climate Dynamics*, Volume 36, Issue 11-12, pp. 2201-2218. 2011. The graph itself is available from http://www.skepticalscience.com/print.php?n=395.

[4] Hathaway, D., and Wilson, R. Geomagnetic activity indicates large amplitude for sunspot cycle 24, a slide. 2006.

[5] Hathaway, D., and Wilson, R. Geomagnetic activity indicates large amplitude for sunspot cycle 24, *Geophysical Research Letters,* 33/11. 2006. Review of the article is provided in http://science.nasa.gov/science-news/science-at-nasa/2006/21dec_cycle24/.

[6] McCracken, K., McDonald, F., Beer, J., Raisbeck, G., Yiou, F. A phenomenological study of the long term cosmic ray modulation, 850-1958 AD. *Journal of Geophysical Research: Space Physics,* 109/A12, 2004.

[7] McInnes, L. Solar activity events in ^{14}C . As of 2014. http://en.wikipedia.org/wiki/File:Carbon14_with_activity_labels.svg.

[8] Scafetta, N. Empirical evidence for a celestial origin of the climate oscillations. *Journal of Atmospheric and Solar-Terrestrial Physics,* 72, pp. 951-970, 2010.

[9] US Geological Survey. Earthquake Archive Search and URL Builder. 2013. http://earthquake.usgs.gov/earthquakes/search/.

[10] US Geological Survey. Magnitude 8 and Greater Earthquakes Since 1900. As of 2014. http://earthquake.usgs.gov/earthquakes/eqarchives/year/mag8/magnitude8_1900_date.php.

[11] Website. Solar activity. As of 2014. http://www.climate4you.com/Sun.htm.